Hopping transport in SrTiO$_3$/Nd$_{1\text{-}x}$TiO$_3$/SrTiO$_3$ heterostructures

Laxman Raju Thoutam,[*] Jin Yue, Peng Xu, and Bharat Jalan[†]

Department of Chemical Engineering and Materials Science, University of Minnesota– Twin Cities, Minneapolis, Minnesota 55455, USA

Electronic transport near the insulator-metal transition is investigated in the molecular beam epitaxy-grown SrTiO$_3$/Nd$_{1\text{-}x}$TiO$_3$/SrTiO$_3$ heterostructures using temperature dependent magnetotransport measurements. It was found that Nd vacancies introduce localized electronic states resulting in variable range hopping transport at low temperatures. At a fixed Nd-vacancy concentration, a crossover from Mott to Efros-Shklovskii variable range hopping transport was observed with decreasing temperature. With increasing disorder, a sign reversal of magnetoresistance from positive to negative was observed revealing interplay between intra-state interaction and the energy dependence of the localization length. These findings highlight the important role of stoichiometry when exploring intrinsic effects using heterostructure and interfaces in addition to offering broad opportunities to tailor low temperature transport using nonstoichiometry defects.

Complex oxides with perovskite structure (ABO_3, where A and B are cations) can host large amounts of disorder including dislocations, strain, and nonstoichiometry such as cation and oxygen vacancies. In particular, cation deficiency can introduce hole-type carriers and compensate for electronic carriers or can even be responsible for forming oxygen vacancies. In valence change oxides, cation vacancies can also be accommodated by valence change. It was recently shown that introduction of Nd vacancies (x) in Nd$_{1\text{-}x}$TiO$_3$/SrTiO$_3$ heterostructures can be accommodated by the change in Ti valence state from Ti$^{3+} \rightarrow$ Ti^{4+}, with a direct consequence on the interfacial conductivity [1]. Cation nonstoichiometry and oxygen vacancies are also argued to play a critical role in realizing two-dimensional electron gas (2DEG) at LaAlO$_3$/SrTiO$_3$ (LAO/STO) interfaces [2–6]. Furthermore, the phenomena such as emerging magnetism, ferroelectricity in complex oxide films, and heterostructures can be influenced by defect-induced disorder [7,8]

Disorder in thin films can come from growth methods, epitaxial strain, interface roughness, and from the choice of growth conditions. Recent density-functional theory study has emphasized the role of growth conditions on the defect formation energy in GdTiO$_3$ that are responsible for the p-type hopping conductivity [9]. The conductivity behavior of these oxides with different disorder level is of practical relevance as these materials are increasingly being investigated for emerging phenomena and for device applications such as Mott transistors.

Variable range hopping (VRH) conduction has long been studied in the context of disordered semiconductors illustrating the temperature dependence of sheet conductance at low temperatures [10]. In a compensated semiconductor, sheet conductance (σ) can follow an exponential behavior:

$$\sigma = \sigma_o \exp\left[-\left(\frac{T_0}{T}\right)^m\right], \qquad (1)$$

where σ_o is a prefactor, T_0 is the characteristic temperature, and m is an exponent. The value of m depends on the type of transport mechanisms. The value of m can be determined using Zabrodskii's analysis, which is an unbiased and quantitative technique that linearizes the conductivity with temperature using a logarithmic derivative method by defining $w = d \ln \sigma / d \ln T$ [11]. The slope of $\ln w$ vs $\ln T$ plot yields m. For nearest neighbor hopping or thermally activated transport, the value of m remains equal to 1 whereas VRH yields a value of 0.25 for 3D Mott VRH, 0.33 for 2D Mott VRH, and 0.5 for Efros-Shklovskii (ES) VRH [12]. The Mott VRH assumes no electron-electron interactions whereas ES VRH accounts for a long range Coulomb interaction [10]. The latter results in the opening of a soft Coulomb gap whose size increases with increasing disorder level (or increasing charge compensation) [10]. For a given density of states, VRH can evolve from the Mott, $T^{-0.25}$, at higher temperature to the ES, $T^{-0.5}$ regime, at low temperature when Mott hopping energy becomes comparable to the ES hopping energy [13]. This crossover has been observed in compensated semiconductors at a fixed disorder level with decreasing temperature, and also by increasing disorder level at a fixed temperature [13]. With decreasing temperature, the conductivity crosses over from the 3D Mott to the ES VRH transport with the crossover temperature given by [13]

$$T_{\text{cross}} = 16 T_{ES}^2 \big/ T_{\text{Mott}}. \qquad (2)$$

In an attempt to understand the role of disorder on transport in Nd$_{1\text{-}x}$TiO$_3$/SrTiO$_3$ heterostructures, we used SrTiO$_3$/Nd$_{1\text{-}x}$TiO$_3$/SrTiO$_3$ heterostructures with varying amount of x. By combining experiment and modeling of low temperature magnetoresistance (MR) measurements in the context of VRH model, we show the carrier transport is primarily governed by the ES VRH and reveals an important role of intrastate correlation between localized sites on the MR behavior.

Three samples consisting of 8 unit cell (u.c.) SrTiO$_3$/2 u.c. Nd$_{1\text{-}x}$TiO$_3$/8 u.c. SrTiO$_3$ heterostructures with varying x were

---

[*]Corresponding author: lthoutam@umn.edu
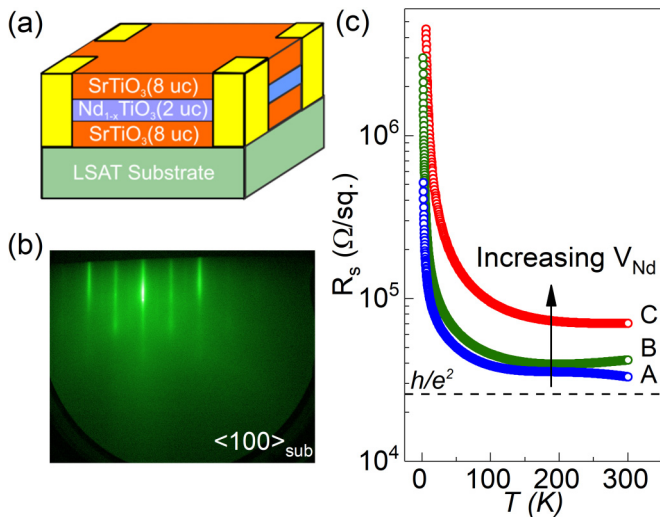
[†]Corresponding author: bjalan@umn.edu

FIG. 1. (a) A schematic of the heterostructure, (b) a representative RHEED pattern of the sample A after growth along the $\langle 100 \rangle$ substrate azimuth, and (c) temperature dependence of R_s for samples A, B, and C with increasing disorder level.

grown on $(La_{0.3}Sr_{0.7})(Al_{0.65}Ta_{0.35})O_3$ (001) substrates using hybrid molecular beam epitaxy method. We have chosen this particular structure in this study because it is well characterized structurally and electronically [1]. Note the stoichiometric 8 u.c. $SrTiO_3$/2 u.c. $Nd_{1-x}TiO_3$/8 u.c. $SrTiO_3$ sample with $x = 0$ gives $1 e^-$/u.c. as is expected from two polar/nonpolar interfaces [1]. Details of the growth method, structure, and stoichiometry optimization are discussed elsewhere [1,14,15]. The value of x was tuned by changing Nd beam equivalent pressure (BEP) during film growth [1]. The Ti and oxygen BEPs were kept fixed. *In situ* reflection high-energy electron diffraction (RHEED) was used to ensure the crystallinity of each layer in the heterostructure prior to the growth of the subsequent layer. 20-nm Al / 20-nm Ti/ 200-nm Au were sputter deposited to make electrical contacts to the sample where Al makes an ohmic contact with the sample. Temperature dependent DC transport measurements were performed in Van der Pauw geometry using Quantum Design Dynacool system. A source-drain current was carefully chosen to ensure ohmic contacts. For MR measurements, magnetic field was swept between -9 T and $+9$ T.

Figures 1(a) and 1(b) show a schematic of the heterostructure and a representative RHEED pattern along $\langle 100 \rangle_{substrate}$ azimuth, respectively. The appearance of the streaky pattern with weak ½-order streaks revealed smooth and crystalline surface morphology. Figure 1(c) shows temperature dependent sheet resistance (R_s) for 8 u.c. $SrTiO_3$/2 u.c. $Nd_{1-x}TiO_3$/8 u.c. $SrTiO_3$ with increasing x from sample A to sample C. It is noted that the increasing x yields larger disorder in $Nd_{1-x}TiO_3$ layer. As shown in Fig. 1(c), the room temperature R_s of sample A and B is near the quantum resistance h/e^2. With increasing x, R_s increases above h/e^2 (sample C) at all temperatures. In particular, for $T < 200$ K, all samples showed an increase in R_s with decreasing T. However, in the more disordered sample C, this resistance upturn appears even at room temperature. In the discussion below, we examine
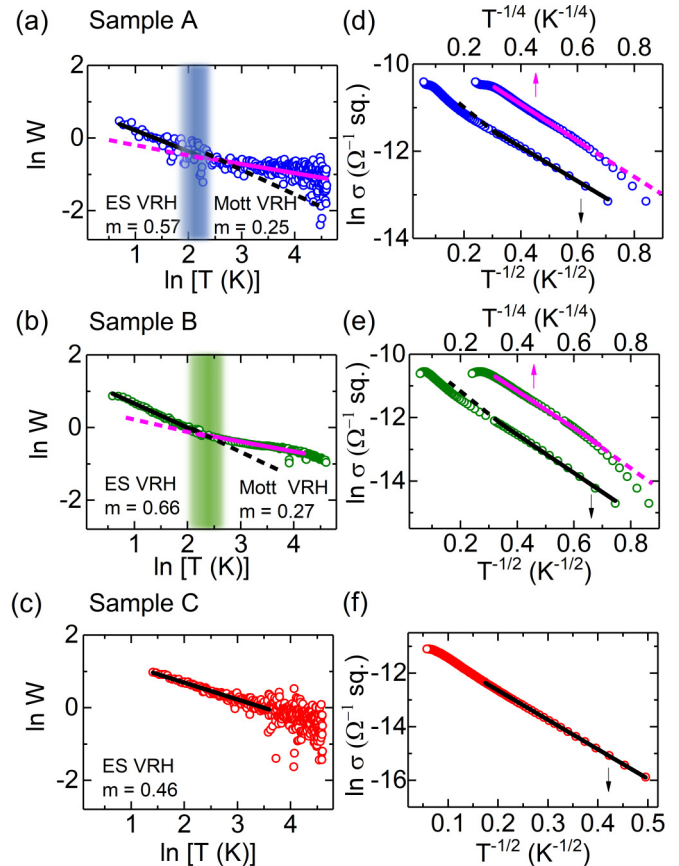

FIG. 2. (a)–(c) Zabrodskii plots of sample A, B, and C. Samples A and B highlight the crossover temperatures between Mott VRH and ES VRH using a vertical shaded region. (d)–(f) $\ln \sigma$ vs T^{-m} plots with linear fits using the m values determined from Zabrodskii's analysis of samples A, B, and C. Arrows in parts (d)–(f) indicate axes.

the origin of resistance upturn at low temperatures and its relationship with disorder that is created intentionally by introducing Nd vacancies.

Figures 2(a)–2(c) illustrate $\ln w$ vs $\ln T$ plots using the Zabrodskii's analysis of sample A, B, and C, respectively. Using the value of exponent m in different temperature ranges determined from these plots, Figs. 2(d)–2(f) show $\ln \sigma$ vs T^{-m} plots with linear fits. We first discuss the results of sample A at a fixed x. Figure 2(a) revealed that the transport in sample A is governed by the ES VRH at $T < 10$ K whereas the Mott 3D VRH mechanism is operative at 10 K $< T < 100$ K with a crossover from ES to Mott VRH at $T_{cross} \simeq 10$ K. The fitting of ES VRH and Mott VRH regime [Fig. 2(d)] yielded $T_{ES} = 15$ K and $T_{Mott} = 311$ K. Using Eq. (2), T_{cross} can be calculated for sample A and is equal to 12 K. The calculated crossover temperature is in excellent agreement with the experimental value as marked by the blue shaded region in Fig. 2(a). A similar crossover behavior from Mott-3D to ES VRH with decreasing temperature was seen previously in In_xO_y [13], n-type CdSe [16], Sr_2IrO_4 [17], and oxygen-deficient ZnO films [18] and is attributed to the formation of a Coulomb gap. The characteristic temperatures T_{Mott} and T_{ES} are defined as $T_{Mott} = 18/k_B N_0(E_F)\xi^3$ and

TABLE I. The characteristic temperatures, T_{Mott} and T_{ES}, calculated and experimental crossover temperatures obtained from the analysis of samples A, B, and C.

Sample	T_{Mott} (K)	T_{ES} (K)	T_{cross} (K) (Experiment)	T_{cross} (K) (Calculated)
A	311	15	∼10	12
B	1139	36	∼15	18
C	–	127	–	–

$T_{ES} = 2.8e^2/\kappa\xi k_B$, where k_B is Boltzmann constant, $N_0(E_F)$ is the density of states at the Fermi level, ξ is the localization length, e is electronic charge, and κ is the dielectric constant [10,12]. The relatively low value of T_{Mott} and T_{ES} in sample A is reasonable given that it is very close to the insulator-metal transition where ξ is expected to diverge to infinity and has been observed previously [13]. The ξ decreases with increasing disorder and therefore increasing disorder is expected to increase T_{cross} [10,13].

Now, we turn to the discussion of the samples B and C, which have higher disorder levels. Sample B yielded a similar Mott 3D VRH to ES VRH crossover and a slightly higher $T_{\text{cross}} = 15$ K. Sample C showed the ES VRH up to T < 45 K. The characteristic temperatures, T_{Mott} and T_{ES}, and the calculated and experimental crossover temperatures obtained from the analysis of samples A, B, and C are listed in Table I. Table I depicts reasonably good agreement between experimental and calculated T_{cross} and reveals larger T_{cross} for sample B with higher disorder. A similar increase in T_{cross} with increased disorder was previously seen in In_xO_y films [13] and is consistent with our results. Sample C yielded much higher $T_{ES} = 127$ K, and is consistent with the increased long range Coulomb interaction in the presence of higher disorder (or more localized sites).

To further understand the interplay between disorder and carrier localization, we performed MR measurements. Figures 3(a)–3(c) show the MR of samples A, B, and C, respectively, as a function of temperature. Sample A showed positive MR at -9 T $\leqslant$ B $\leqslant +9$ T whose magnitude increases with decreasing temperature in the measured temperature range. Likewise, sample B showed a positive MR at low fields but a negative MR at higher fields. It was also found that the crossover field at which MR changes its sign decreases as temperature decreases. Sample C exhibited only negative MR at all fields. Overall, these results revealed that the MR undergoes a sign reversal from positive to negative with increasing disorder from sample A to sample C. A similar trend was observed with increasing magnetic field in sample B with intermediate disorder level. These results are illustrated in Fig. 3(d) at a fixed temperature, 10 K.

We now discuss the MR results. The MR in the VRH regime can be both positive and negative. Positive MR in the VRH regime can result from shrinkage of carrier wave function with increasing field [10,19–21] or could be due to the intrastate correlation of carriers in the localized states [22–24]. Kurobe and Kamimura have proposed a model accounting for intrastate correlation of spins in hopping sites that could give rise to the positive MR [24]. Using their
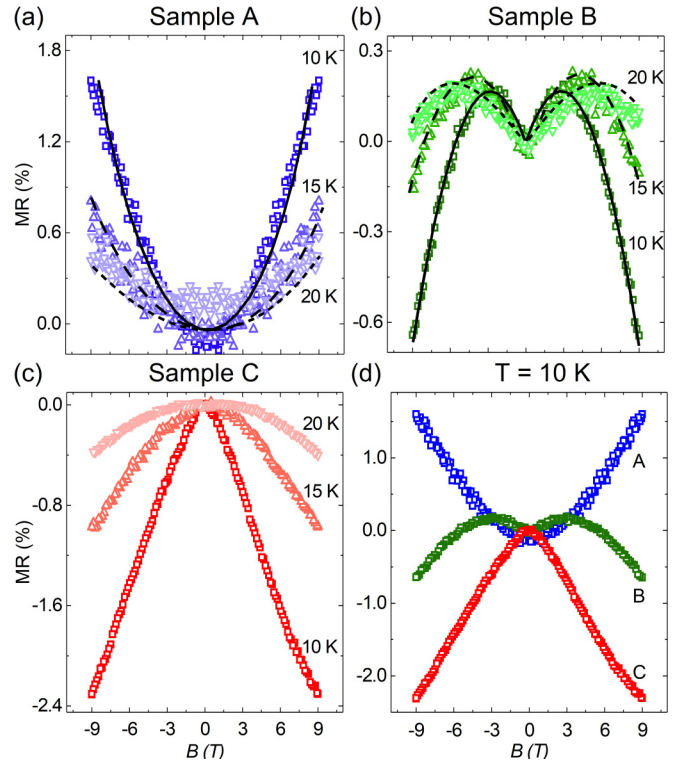

FIG. 3. Normalized MR at 20, 15, and 10 K for (a) sample A, (b) sample B, and (c) sample C, (d) comparison of MR at 10 K revealing a sign reversal from positive to negative values with increasing disorder from sample A to sample C. Black solid lines are guide to the eyes.

numerical results, Frydman and Ovadyahu later proposed a simple analytical formula [25]. This model corroborates very well with our measurements (discussed later). According to this model, the density of states in systems with intrastate correlation (in the presence of large disorder) can be thought of in terms of an unoccupied state (UO), singly occupied state (SO), and doubly occupied state (DO) at the Fermi level. Consequently, four types of hopping processes can be possible viz., SO to UO, SO to SO, DO to UO and DO to SO contributing to hopping probability in the absence of any external magnetic field as schematically illustrated in Fig. 4(a). For illustration, we only show SO → UO and SO → SO hopping processes. Applying a magnetic field aligns local spins and thus reduces the hopping probability between sites as depicted using a red cross in Fig. 4(b) for SO → SO hopping. This behavior, in turn, results in the positive MR followed by the saturation when all spins are aligned [24–26]. We note that this model does not take into account the state-energy dependence of localization length [24]. According to this model, the positive MR or negative magnetoconductance (MC = $\frac{\Delta\sigma}{\sigma} = \frac{\sigma(H)-\sigma(0)}{\sigma(0)}$) is given by [25]

$$\frac{\Delta\sigma}{\sigma} = -A_e \frac{H^2}{H^2 + H_e^2} , \qquad (3)$$

where A_e is the saturation value, $H_e = a\frac{k_B T}{\mu_B}(\frac{T_{\text{Mott}}}{T})^{0.5}$ is the spin alignment field, a is the constant of the order unity, k_B is the Boltzmann constant, and μ_B is the Bohr magneton.
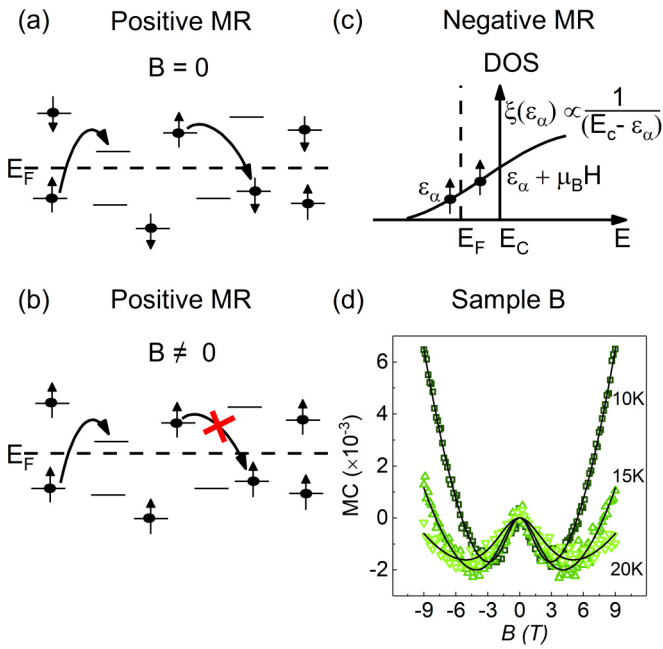
FIG. 4. Schematic illustration of the mechanism responsible for the positive MR at (a) $B = 0$ and (b) $B \neq 0$. Red cross in (b) shows the transition between SO → SO localized states is energetically not possible due to spin alignment, (c) schematic illustration of the mechanism for negative MR showing an arbitrary DOS vs energy diagram. A formula describing the relationship between ξ and $E_c - \varepsilon_\alpha$ is included where ε_α is the state energy of the localized electron in a SO state, E_c is the mobility edge, and E_F is the Fermi level. Black solid circles with an up-arrow show state energies of a localized electron in the absence and presence of applied field B, with reference to the Fermi energy, (d) temperature dependent magnetoconductance (MC) of sample B. Solid black lines are fits to the experimental data.

Negative MR in VRH can arise from the orbital quantum interference effect or the state-energy dependence of ξ in the presence of an applied magnetic field [27–31]. The main evidence of the former comes from the presence of anisotropic MR with the field in-plane and out-of-plane of the sample [31]. Figure S1 shows the isotropic negative MR of sample C with both in-plane and out-of-plane field directions and suggests the orbital quantum interference mechanism is not operative here [32]. As for the dependence of field on ξ, Fukuyama and Yoshida proposed a model explaining the negative MR in the VRH regime [27]. Schematically, we illustrate this model in Fig. 4(c), which shows an arbitrary density of states dependence of ξ on $E_c - \varepsilon_\alpha$ [i.e., $\xi(\varepsilon_\alpha) \propto 1/(E_c - \varepsilon_\alpha)$], where ε_α is state energy of the localized electron in a SO state,

the mobility edge (E_c), and the Fermi level (E_F). It is argued that an application of field can decrease electron energy by $g\mu_B H$ (g is the Lande factor, and H is the magnetic field) according to the Zeeman effect such that $E_f = \varepsilon_\alpha - g\mu_B H$, resulting in the increase of ξ, and therefore, a negative MR [24,27]. According to the Fukuyama and Yoshida model, the negative MR or the positive MC is given by [27]

$$\frac{\Delta\sigma}{\sigma} = c\left(\frac{g\mu_B H}{E_c - E_F}\right)^2 \left(\frac{T_{\mathrm{Mott}}}{T}\right)^{0.5}, \qquad (4)$$

where c is a constant and is equal to unity. Equations (3) and (4) explain our measurements of positive and negative MR, respectively, in sample A and C. Figure 4(d) shows the MC from the measured MR data of sample B as depicted in Fig. 3(b). Fittings to the experimental MC data are also included as black solid lines using an equation comprised of the summation of Eqs. (3) and (4). Our observed MC behavior is quantitatively in excellent agreement with these models. A similar positive and negative MR behavior based on correlation effect has been previously studied both theoretically [28,29] and experimentally in other systems including Cu-particle films [30], heavily $FeCl_3$-doped polyacetylene [33], and more recently, in $SmNiO_3$ [34]. Future investigations will focus on detailed quantitative analysis of these MR behaviors.

In summary, electronic transport in $SrTiO_3/Nd_{1-x}TiO_3/SrTiO_3$ heterostructures is performed in the insulating regime near the insulator-metal transition boundary as a function of Nd vacancies. Temperature dependent transport revealed Mott to ES VRH transition with a crossover temperature in excellent agreement with the calculated crossover temperatures. With increasing disorder, films exhibited ES VRH transport and negative MR. The analysis of MR revealed an important interplay between the intrastate correlation effect and magnetic field dependent localization length as a function of disorder and magnetic field. We argue that such insights might be useful in further studies of intrinsic phenomena in oxide heterostructures as well as in comparing materials grown using different synthesis approaches.

[1] P. Xu, Y. Ayino, C. Cheng, V. S. Pribiag, R. B. Comes, P. V. Sushko, S. A. Chambers, and B. Jalan, Phys. Rev. Lett. **117**, 106803 (2016).

[2] M. P. Warusawithana, C. Richter, J. A. Mundy, P. Roy, J. Ludwig, S. Paetel, T. Heeg, A. A. Pawlicki, L. F. Kourkoutis, M. Zheng, M. Lee, B. Mulcahy, W. Zander, Y. Zhu, J.

Schubert, J. N. Eckstein, D. A. Muller, C. S. Hellberg, J. Mannhart, and D. G. Schlom, Nat. Commun. **4**, 2351 (2013).

[3] C. Weiland, G. E. Sterbinsky, A. K. Rumaiz, C. S. Hellberg, J. C. Woicik, S. Zhu, and D. G. Schlom, Phys. Rev. B **91**, 165103 (2015).

[4] E. Breckenfeld, N. Bronn, J. Karthik, A. R. Damodaran, S. Lee, N. Mason, and L. W. Martin, Phys. Rev. Lett. **110**, 196804 (2013).

[5] L. Yu and A. Zunger, Nat. Commun. **5**, 5118 (2014).

[6] D. G. Schlom and J. Mannhart, Nat. Mater. **10**, 168 (2011).

[7] Y. Ayino, P. Xu, J. T-Lazo, J. Yue, B. Jalan, and V. S. Pribiag, Phys. Rev. Mater. **2**, 031401(R) (2018).

[8] H. W. Jang, A. Kumar, S. Denev, M. D. Biegalski, P. Maksymovych, C. W. Bark, C. T. Nelson, C. M. Folkman, S. H. Baek, N. Balke, C. M. Brooks, D. A. Tenne, D. G. Schlom, L. Q. Chen, X. Q. Pan, S. V. Kalinin, V. Gopalan, and C. B. Eom, Phys. Rev. Lett. **104**, 197601 (2010).

[9] L. Bjaalie, A. Janotti, K. Krishnaswamy, and C. G. Van de Walle, Phys. Rev. B **93**, 115316 (2016).

[10] B. I. Shklovskii and A. L. Efros, *Electronic Properties of Doped Semiconductors* (Springer, Berlin, 1984).

[11] A. G. Zabrodskii and K. N. Zinoveva, Zh. Eksp. Teor. Fiz. **86**, 727 (1984) [Sov. Phys. JETP **37**, 727 (1983)].

[12] N. F. Mott and E. A. Davis, *Electronic Processes in Non-Crystalline Materials*, 2nd ed. (Clarendon, Oxford, 1979).

[13] R. Rosenbaum, Phys. Rev. B **44**, 3599 (1991).

[14] P. Xu, T. C. Droubay, J. S. Jeong, K. A. Mkhoyan, P. V. Sushko, S. A. Chambers, and B. Jalan, Adv. Mater. Interfaces **3**, 1500432 (2016).

[15] P. Xu, D. Phelan, J. S. Jeong, K. A. Mkhoyan, and B. Jalan, App. Phys. Lett. **104**, 082109 (2014).

[16] Y. Zhang, O. Dai, M. Levy, and M. P. Sarachik, Phys. Rev. Lett. **64**, 2687 (1990).

[17] C. Lu, A. Quindeau, H. Deniz, D. Preziosi, D. Hesse, and M. Alexe, Appl. Phys. Lett. **105**, 082407 (2014).

[18] Y. L. Huang, S. P. Chiu, Z. X. Zhu, Z. Q. Li, and J. J. Lin, J. Appl. Phys. **107**, 063715 (2010).

[19] M. Pollak and B. Shklovskii, *Hopping Transport in Solids* (Elsevier, North-Holland, 1991).

[20] Z. Ovadyahu, in *Hopping and Related Phenomena*, edited by H. Fritzsche and M. Pollak (World Scientific, Singapore, 1990), Vol. 2, pp. 193–206.

[21] W. Jiang, J. L. Peng, J. J. Hamilton, and R. L. Greene, Phys. Rev. B **49**, 690 (1994).

[22] A. L. Efros and M. Pollak, *Electron-Electron Interactions in Disordered Systems* (North-Holland, Amsterdam, 1985).

[23] P. Bhattacharya, R. Fornari, and H. Kamimura, *Comprehensive Semiconductor Science and Technology* (Elsevier Science, Amsterdam, 2011).

[24] A. Kurobe and H. Kamimura, J. Phys. Soc. Jpn. **51**, 1904 (1982).

[25] A. Frydman and Z. Ovadyahu, Solid State Commun. **94**, 745 (1995).

[26] H. Kamimura and H. Aoki, *The Physics of Interacting Electrons in Disordered Systems* (Clarendon Press, Oxford, 1989).

[27] H. Fukuyama and K. Yoshida, J. Phys. Soc. Jpn. **46**, 102 (1979).

[28] M. Eto, Phys. Rev. B **48**, 4933 (1993).

[29] M. Eto, Phys. Rev. B **51**, 13066 (1995).

[30] J. J. Lin, R. Yamada, and S. Kobayashi, J. Phys. Soc. Jpn. **63**, 4514 (1994).

[31] F. Tremblay, M. Pepper, R. Newbury, D. Ritchie, D. C. Peacock, J. E. F. Frost, G. A. C.Jones, and G. Hill, Phys. Rev. B **40**, 10052 (1989).

[32] See Supplemental Material at http://link.aps.org/supplemental/10.1103/PhysRevMaterials.3.065006 for the MR measurements of sample C with both in-plane and out-of-plane field directions.

[33] H. Kaneko, T. Ishiguro, J. Tsukamoto, and A. Takahashi, Solid State Commun. **90**, 83 (1994).

[34] K. Ramadoss, N. Mandal, X. Dai, Z. Wan, Y. Zhou, L. Rokhinson, Y. P. Chen, J. Hu, and S. Ramanathan, Phys. Rev. B **94**, 235124 (2016).